Loss-compensated nonlinear modes and symmetry breaking in amplifying metal-dielectric-metal plasmonic couplers

Andrea Marini,[1,*] Samudra Roy,[2] Ajit Kumar,[3] and Fabio Biancalana[4,5]
[1]*ICFO-Institut de Ciencies Fotoniques, Mediterranean Technology Park, E-08860 Castelldefels (Barcelona), Spain*
[2]*Department of Physics, Indian Institute of Technology, Kharagpur-721302, India*
[3]*Department of Physics, Indian Institute of Technology, Hauz Khas, New Delhi 110016, India*
[4]*Max Planck Institute for the Science of Light, Guenther-Scharowsky-Straße 1, D-91058 Erlangen, Germany*
[5]*School of Engineering & Physical Sciences, Heriot-Watt University, Edinburgh, EH14 4AS, United Kingdom*
(Received 18 January 2015; published 9 April 2015)

We theoretically investigate the propagation of surface plasmon polaritons in an amplifying plasmonic coupler (metal–amplifying dielectric–metal). We study the loss-compensated nonlinear stationary modes of the system by deriving coupled-mode equations for the optical amplitudes, predicting the existence of a mode with broken symmetry for gain values higher than a characteristic threshold. We analyze the stability of symmetric, antisymmetric, and nonsymmetric modes by solving the linearized system for small perturbations and by numerically integrating coupled-mode equations in propagation. We find that, while the antisymmetric mode stays always stable or marginally stable, the stability of symmetric and nonsymmetric modes is more involved.

DOI: 10.1103/PhysRevA.91.043815 PACS number(s): 42.65.Tg, 73.20.Mf, 42.65.Wi

I. INTRODUCTION

Plasmonics is one of the most developing research areas of physics and aims at controlling and manipulating light at the nano-scale. If plasmons—collective oscillations of electrons—are coupled to the electromagnetic field nearby the surface of a metal, exponentially localized surface plasmon polariton (SPP) modes can be excited [1]. SPPs can confine light in the subwavelength scale overcoming the natural limit of light diffraction and are used as optical interconnects in highly integrated optoelectronic circuits [2]. In addition, they are responsible for several effects including extraordinary optical transmission through subwavelength hole arrays [3], perfect imaging [4], and giant enhancement of local fields [5]. In particular, the latter mechanism boosts all the nonlinear processes [6], which can be exploited in several applications, e.g., biosensing [7], ultrafast processing of optical signals [8], and plasmon-soliton formation [9–11]. Besides, nonlinearity can be exploited to achieve symmetry breaking and switching in plasmonic arrays and couplers, thus enabling all-optical control and manipulation of SPPs [12–17]. However, the above mentioned applications are hampered by the presence of large intrinsic ohmic losses of metals that damp the optical signal [18]. In turn, several strategies have been proposed to retain the subwavelength localization provided by SPPs and overcome the loss barrier of metals, e.g., the suppression of interband absorption through ultrashort self-induced transmitted plasmon solitons [19]. Besides, substantial research has been addressed to the study of plasmonic devices embedding gaining media [20,21]. After the seminal discovery of stimulated emission of localized surface plasmons [22], amplification of SPPs has been theoretically predicted [23] and experimentally observed in several setups, e.g., using erbium ions [24], rhodamine [25], PbS (Lead sulfide) quantum dots [26], and hybrid organic-inorganic polymers [27]. In particular, the intrinsic nonlinearity of two-level gaining media enables stationary propagation of SPPs [28] and transverse localization of dissipative plasmon solitons [29,30]. In this context, the effect of metal nonlinearities [31–34] can be disregarded, as the gaining two-level system is resonant and its saturated nonlinearity plays a major role.

In this paper, we investigate SPP propagation in an amplifying plasmonic coupler (metal–amplifying dielectric–metal). We analyze the loss-compensated nonlinear stationary modes of the system by deriving coupled-mode equations for the left and right SPP amplitudes of the coupler. We demonstrate the existence of three kinds of stationary dissipative modes: symmetric, antisymmetric, and nonsymmetric modes, which exist for gain values higher than a characteristic threshold. The stability analysis shows that for zero detuning symmetric or antisymmetric modes are marginally stable while nonsymmetric modes are unstable. For negative detuning, we find that antisymmetric modes are stable while symmetric modes are unstable within a short range of gain values and stable elsewhere. Conversely, nonsymmetric modes are stable only within a short range of gain values and unstable elsewhere. We confirm our predictions by integrating the coupled-mode equations in propagation.

The paper is organized as follows: In Sec. II we describe the physical setup under consideration, the transverse magnetic (TM) Maxwell equations for SPPs, and the loss-compensated linear modes of the system; in Sec. III we develop a coupled-mode theory for right and left SPPs of the coupler and we study the loss-compensated nonlinear stationary modes of the system (accounting for gain saturation) and their stability.

II. SETUP

In the following we consider an amplifying plasmonic coupler, composed of a transparent amplifying medium embedded between two thick silver slabs; the setup is sketched in Fig. 1. SPPs propagate along the z direction and are exponentially localized along the x direction at the two silver-dielectric interfaces $x = \pm a$. Gain is provided

*andrea.marini.tlp@gmail.com

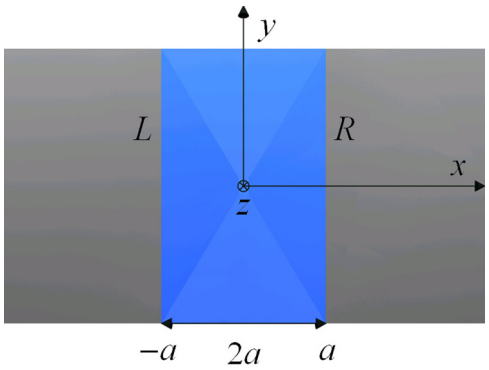

FIG. 1. (Color online) Illustrative sketch of the structure analyzed in this work: a silver-based amplifying plasmonic coupler supporting SPPs at every z-y interface. The dielectric medium (center blue slab) embeds externally pumped active inclusions, which amplify SPPs propagating along the z direction. The dielectric slab of width $2a$, sandwiched between two thick silver slabs, supports SPPs at the left and right interfaces with optical amplitudes L, R. The system is assumed homogeneous in the y,z directions and the silver slabs are assumed infinitely extended in the x direction.

by externally pumped active inclusions embedded in the sandwiched dielectric layer that can be modeled as a two-level system. For continuous monochromatic waves oscillating with angular frequency ω, the complex susceptibility ϵ_D of the amplifying dielectric medium is inherently nonlinear [29]: $\epsilon_D = \epsilon_b + \alpha(\delta - i)/(1 + \delta^2 + |\mathcal{E}/E_S|^2)$, where ϵ_b is the linear permittivity of the hosting medium, α is the dimensionless gain (rescaled to ω/c), c is the speed of light in vacuum, δ is the dimensionless detuning from resonance ω_R rescaled to the dephasing rate T_2^{-1} [$\delta = T_2(\omega - \omega_R)$], E_S is the saturation field, and $\mathcal{E}e^{-i\omega t}$ is the electric field of the optical wave. SPP propagation is governed by Maxwell equations for TM waves:

$$\partial_{xz}^2 \mathcal{E}_z - \partial_{zz}^2 \mathcal{E}_x = \mathcal{D}_x/\epsilon_0, \tag{1}$$

$$\partial_{xz}^2 \mathcal{E}_x - \partial_{xx}^2 \mathcal{E}_z = \mathcal{D}_z/\epsilon_0, \tag{2}$$

where ϵ_0 is the vacuum dielectric permittivity, x,z are the dimensionless spatial coordinates [rescaled to $(\omega/c)^{-1}$], $\mathcal{E} = (\mathcal{E}_x \mathcal{E}_z)^T$ is the electric field, and $\mathcal{D} = (\mathcal{D}_x \mathcal{D}_z)^T = \epsilon_0 \epsilon(x)\mathcal{E} + \mathcal{P}_{\rm NL}$ is the displacement vector. Note that ∂_y derivatives do not appear as the system is assumed infinitely extended in the y direction. The linear permittivity profile is $\epsilon(x) = \epsilon_m \theta(|x| - a) + \epsilon_d \theta(a - |x|)$, where $2a$ is the thickness of the dielectric layer, $\theta(x)$ is the Heaviside step function, $\epsilon_m = \epsilon_m' + i\epsilon_m''$ is the dielectric constant of silver, and $\epsilon_d = \epsilon_b + \alpha(\delta - i)/(1 + \delta^2)$ is the linear permittivity of the gain medium. The nonlinear polarization $\mathcal{P}_{\rm NL} = \epsilon_0(\epsilon_D - \epsilon_d)\theta(a - |x|)\mathcal{E}$ accounts for gain saturation and focusing or defocusing nonlinearity of the gain medium:

$$\mathcal{P}_{\rm NL} = \frac{\epsilon_0 \alpha(i - \delta)|\mathcal{E}/E_S|^2 \mathcal{E}}{(1 + \delta^2)(1 + \delta^2 + |\mathcal{E}/E_S|^2)} \theta(a - |x|). \tag{3}$$

A. Loss-compensated linear modes

For weak optical fields much smaller than the saturation field, gain saturation and focusing or defocusing nonlinearity (accounted for by the nonlinear polarization $\mathcal{P}_{\rm NL}$) can be neglected. In this section we find the linear modes of the system by taking the Ansatz $\mathcal{E}(x,z) = \mathcal{A}\mathbf{e}(x)e^{i\beta z}$, where $\mathcal{A}$ is the arbitrary mode amplitude, $\mathbf{e}(x)$ is the dimensionless mode profile, and β is its corresponding propagation constant. In this weak intensity limit, Maxwell equations for TM modes reduce to

$$\beta^2 e_x + i\beta \partial_x e_z = \epsilon(x) e_x, \tag{4}$$

$$i\beta \partial_x e_x - \partial_{xx}^2 e_z = \epsilon(x) e_z, \tag{5}$$

with the boundary conditions (BCs): $\epsilon_m e_x(-a^-) = \epsilon_d e_x(-a^+)$, $\epsilon_d e_x(a^-) = \epsilon_m e_x(a^+)$, $e_z(\pm a^-) = e_z(\pm a^+)$. Besides, as we are looking for guided modes, we require that $|\mathbf{e}| \to 0$ for $x \to \pm\infty$. Under these constraints, Eqs. (4) and (5) provide two solutions with opposite symmetry:

$$e_x = \frac{i\beta(q_d\epsilon_m + q_m\epsilon_d)}{2q_d q_m \epsilon_d e^{-q_d a}} [e^{q_d x} \pm e^{-q_d x}]\theta(a - |x|) + \frac{i\beta}{q_m} e^{q_m a} \left[e^{q_m x}\theta(-x - a) \pm e^{-q_m x}\theta\left(x - \frac{a}{2}\right)\right], \tag{6}$$

$$e_z = \frac{(q_d\epsilon_m + q_m\epsilon_d)}{2q_m \epsilon_d e^{-q_d a}} [\pm e^{-q_d x} - e^{q_d x}]\theta(a - |x|) + e^{q_m a}[\pm e^{-q_m x}\theta(x - a) - e^{q_m x}\theta(-x - a)], \tag{7}$$

where $q_{d,m}^2 = \beta^2 - \epsilon_{d,m}$, and the propagation constant β satisfies the dispersion relation:

$$e^{2q_d a} = \pm \frac{q_d\epsilon_m - q_m\epsilon_d}{q_d\epsilon_m + q_m\epsilon_d}. \tag{8}$$

Note that the symmetries of longitudinal (e_z) and transverse (e_x) electric field components are opposite. In what follows, we refer to symmetric or antisymmetric modes as the modes where the longitudinal component e_z is symmetric or antisymmetric (while e_x is antisymmetric or symmetric).

The dimensionless propagation constant β is a complex quantity: Its real part β' accounts for the SPP phase shift while its imaginary part β'' accounts for damping ($\beta'' > 0$) or gain ($\beta'' < 0$) depending on the net balance between the ohmic losses of silver and the amplification provided by the externally pumped active inclusions embedded in the dielectric slab. Amplification basically depends on the gain parameter α, which can be tuned by changing the external pumping power. We denote by α_0 the amplification threshold, where $\beta'' = 0$ and stationary SPPs propagate in the coupler. We have numerically calculated the amplification threshold α_0 and the corresponding phase shift (effective index) $n_{\rm eff} = \beta'$. In Fig. 2(a), we plot the effective index and in Fig. 2(b) the gain threshold of the symmetric (solid blue lines) and antisymmetric (dashed red lines) modes versus the slab thickness $2a$. The black dotted lines represent (a) the effective index and (b) the gain threshold of a single interface between silver and the gaining medium. In our calculations we have assumed that the gaining medium is rhodamine 6G (embedded within a polymer matrix), operating at the resonant wavelength $\lambda = 530$ nm (assuming zero detuning: $\delta = 0$). The dielectric constant of the hosting dielectric medium (polymer) was assumed $\epsilon_b = 1.8$, while the dielectric constant of silver at

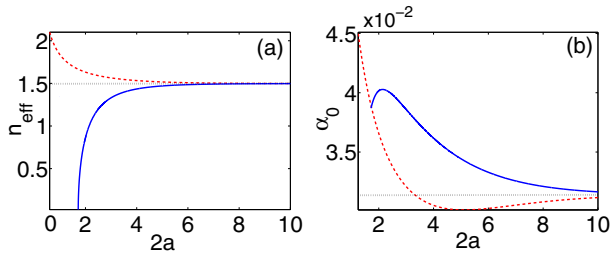

FIG. 2. (Color online) (a) Effective index $n_{\rm eff}$ and (b) amplification threshold α_0 as functions of the dielectric slab thickness $2a$. Solid blue (dashed red) lines represent symmetric (antisymmetric) modes (the symmetry refers to the longitudinal field component e_z). The black dotted lines represent (a) the effective index and (b) the gain threshold of a single interface between silver and the gaining medium. In our calculations we have assumed $\lambda = 530$ nm, $\epsilon_m = -9 + 0.8i$, $\delta = 0$, and $\epsilon_b = 1.8$.

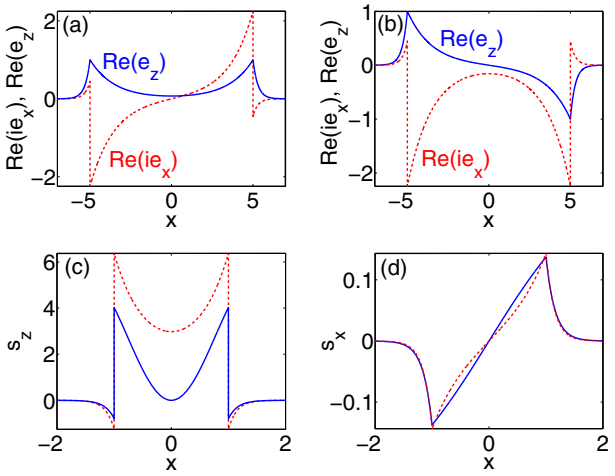

FIG. 3. (Color online) (a) and (b) Profiles of (a) symmetric and (b) antisymmetric modes for $a = 5$. Solid blue (dashed red) lines represent the real part of the longitudinal Re(e_z) [transverse Re(ie_x)] components of the symmetric or antisymmetric modes. (c) and (d) Profiles of the (c) longitudinal (s_z) and (d) transverse (s_x) components of the dimensionless Poynting vector ($\mathbf{s}$) for $a = 1$. Solid blue (dashed red) lines represent symmetric (antisymmetric) modes. Other parameters used in our calculations coincide with the ones used in Fig. 3.

$\lambda = 530$ nm is $\epsilon_m = -9 + 0.8i$ [35]. The slab thickness is expressed in dimensionless units [the physical thickness is $2a(\omega/c)^{-1}$]. Note that, when the slab thickness is smaller than $2a \simeq 2$, the symmetric mode is cut off. When $2a \simeq 10$, SPPs at the two left and right interfaces are almost uncoupled, and both the effective index $n_{\rm eff}$ and the amplification threshold α_0 converge to the single-interface results. While in the fully coupled case $a \approx 1$ the dispersion relation is given by a transcendent equation, in the limit of small coupling $a \gg 1$, it is given by the simpler expression $\beta = \sqrt{\epsilon_d \epsilon_m/(\epsilon_d + \epsilon_m)}$, and the amplification threshold is

$$\alpha_0 = \frac{1}{2\epsilon_m''}(|\epsilon_m|^2 - 2\epsilon_m''\epsilon_b\delta) + \\ -\frac{1}{2\epsilon_m''}\sqrt{|\epsilon_m|^4 - 4\epsilon_m''\epsilon_b(\epsilon_m''\epsilon_b + \delta|\epsilon_m|^2)}. \quad (9)$$

In Figs. 3(a) and 3(b), we depict the structure of the symmetric (a) and the antisymmetric (b) modes for $a = 5$, $\lambda = 530$ nm, $\epsilon_m = -9 + 0.8i$, $\delta = 0$, and $\epsilon_b = 1.8$. Solid blue [dashed red] lines represent the real part of the longitudinal Re(e_z) [transverse Re(ie_x)] components of the symmetric or antisymmetric modes. Note that these modes are stationary, as gain provided by the amplifying dielectric compensates for ohmic losses of silver. In turn, phase is not conserved in the x direction and the imaginary parts of the mode components [Im(ie_x), Ime_z] are also x dependent. Indeed, this phase flow accounts for the exact power transfer (in the x direction) from the amplifying medium to the surrounding silver that is necessary for stationary propagation to occur. The longitudinal or transverse power transfer in the z/x directions is described by the Poynting vector:

$$\mathbf{S} = S_x\hat{x} + S_z\hat{z} \\ = \frac{1}{2}\mathrm{Re}[\mathcal{E} \times \mathcal{H}^*] = \frac{|\mathcal{A}|^2}{2c\mu_0}\mathrm{Re}[-h_y^* e_z\hat{x} + h_y^* e_x\hat{z}], \quad (10)$$

where $\mathcal{H}$ is the magnetic field in the y direction, μ_0 is the vacuum magnetic permeability, $\hat{x},\hat{z}$ are the x,y unit vectors, and $h_y = \beta e_x + i\partial_x e_z$. In turn, apart from the arbitrary dimensional factor $|\mathcal{A}|^2/(2c\mu_0)$, the x-dependent profile of the Poynting vector is accounted for by the dimensionless quantity,

$$\mathbf{s} = s_x\hat{x} + s_z\hat{z} = \mathrm{Re}[-h_y^* e_z\hat{x} + h_y^* e_x\hat{z}]. \quad (11)$$

In Figs. 3(c) and 3(d), we depict the structure of (c) longitudinal (s_z) and (d) transverse (s_x) components of the dimensionless Poynting vector ($\mathbf{s}$) for $a = 1$, $\lambda = 530$ nm, $\epsilon_m = -9 + 0.8i$, $\delta = 0$, and $\epsilon_b = 1.8$. Solid blue (dashed red) lines represent symmetric (antisymmetric) modes. The longitudinal component s_z is symmetric for both symmetric and antisymmetric modes: It is positive within the amplifying dielectric (forward propagation) and negative in the outer silver (backward propagation). However, the power density $p_z = \int_{-\infty}^{+\infty} s_z dx$ stays positive and SPPs effectively propagate in the forward direction. The transverse component s_x is antisymmetric for both symmetric and antisymmetric modes, meaning that for these stationary modes there exists an outward power flow from the center of the amplifying medium ($x = 0$) towards the outer metal regions ($|x| > a$).

III. COUPLED-MODE THEORY

When the thickness of the dielectric slab is much longer than the field penetration depth ($a \gg 1$), the field overlap and the resulting coupling between adjacent SPPs at left and right interfaces are small. In turn, for weak optical fields much smaller than the saturation field ($|\mathcal{E}| \ll E_S$) optical propagation can be modeled in terms of coupled-mode equations (CMEs) [14,36]. In this limit, the full-saturated dielectric permittivity of the gaining medium can be approximated by its first-order Taylor expansion in terms of $|\mathcal{E}/E_S|^2$: $\epsilon_D \simeq \epsilon_b + \Delta\epsilon_d + \chi_3|\mathcal{E}|^2$, where $\Delta\epsilon_d = \alpha(\delta - i)/(1 + \delta^2)$ accounts for linear gain and phase shift, while the third-order susceptibility $\chi_3 = \alpha(i - \delta)/(E_S + \delta^2 E_S)^2$

accounts for focusing or defocusing nonlinearity (depending on the sign of the detuning δ) and nonlinear saturation of the gain. Thus, the linear dielectric permittivity can be expressed as the sum $\epsilon(x) = \epsilon_A(x) + \Delta\epsilon(x)$, where $\epsilon_A(x) = \epsilon'_m\theta(|x| - a) - \epsilon_b\theta(a - |x|)$ and $\Delta\epsilon(x) = i\epsilon''_m\theta(|x| - a) + \Delta\epsilon_d\theta(a - |x|)$. Besides, the nonlinear polarization is approximated by $\mathcal{P}_{\rm NL} \approx \epsilon_0\chi_3|\mathcal{E}|^2\mathcal{E}\theta(a - |x|)$.

CMEs are derived through a multiple-scale expansion, by assuming that the effects of metal losses and of the active inclusions embedded in the dielectric medium are small: $|\Delta\epsilon\mathcal{E}|, |\mathcal{P}_{\rm NL}/\epsilon_0| \ll |\epsilon_A\mathcal{E}|$. Introducing the small dummy variable s, we make the following Ansatz:

$$\mathcal{E} = E_S[L(z)\mathbf{e}_L(x) + R(z)\mathbf{e}_R(x) + \Delta\mathbf{E}]e^{i\beta_0 z} + o(s^{5/2}), \tag{12}$$

where $\mathbf{e}_{L,R}$ are the unperturbed mode profiles of left and right interfaces, L, R are the left and right mode amplitudes, β_0 is the unperturbed propagation constant, and $\Delta\mathbf{E}$ is the residual field correction. For the development of the multiscale expansion we assume that

$$|L|, |R| \sim o(s^{1/2}), \quad |\Delta\epsilon|, e^{-2q_d a} \sim o(s), \tag{13}$$

$$|\partial_z L|, |\partial_z R|, |\Delta\mathbf{E}| \sim o(s^{3/2}). \tag{14}$$

The left and right SPP amplitudes $L(z), R(z)$ and mode profiles $\mathbf{e}_{L,R}$ are dimensionless, while the physical dimensions are carried by the saturation field E_S. The assumption that $e^{-2q_d a}$ is small and of the same order of $|\Delta\epsilon|$ states quantitatively the approximation of weak overlap between adjacent SPPs.

A. Linear modes and dispersion: $o(s^{1/2})$ order

At the $o(s^{1/2})$ order, left (L) and right (R) SPPs are uncoupled. Inserting the Ansatz given by Eq. (12) in Eqs. (1) and (2) one gets the linear system of differential equations $\hat{\mathcal{L}}_k\mathbf{e}_k = 0$, where the labels $k = L, R$ correspond to left and right SPPs, $\mathbf{e}_k$ are the uncoupled linear mode profiles $\mathbf{e}_k = (e_{k,x}e_{k,z})^T$, and

$$\hat{\mathcal{L}}_k = \begin{pmatrix} \beta_0^2 - \epsilon_k & i\beta_0\partial_x \\ i\beta_0\partial_x & -\epsilon_k - \partial_{xx}^2 \end{pmatrix}. \tag{15}$$

The unperturbed dielectric permittivity profiles $\epsilon_k(x) = \epsilon_{L,R}(x)$ represent single isolated left and right interfaces and are explicitly given by $\epsilon_L = \epsilon'_m\theta(-x - a) + \epsilon_b\theta(x + a)$, $\epsilon_R = \epsilon'_m\theta(x - a) + \epsilon_b\theta(-x + a)$. BCs at $o(s^{1/2})$ order require the continuity of $e_{k,z}$ and $\epsilon_k e_{k,x}$ at the interfaces $x = \pm a$. In turn, solving the linear system $\hat{\mathcal{L}}_k\mathbf{e}_k = 0$ and using the BCs above one gets

$$\mathbf{e}_L(x) = \begin{pmatrix} \frac{i\beta_0}{q_d} \\ 1 \end{pmatrix} e^{-q_d(x+a)}\theta(x + a) + \begin{pmatrix} -\frac{i\beta_0}{q_m} \\ 1 \end{pmatrix} e^{q_m(x+a)}\theta(-x - a), \tag{16}$$

$$\mathbf{e}_R(x) = \begin{pmatrix} \frac{i\beta_0}{q_m} \\ 1 \end{pmatrix} e^{-q_m(x-a)}\theta(x - a) + \begin{pmatrix} -\frac{i\beta_0}{q_d} \\ 1 \end{pmatrix} e^{q_d(x-a)}\theta(-x + a), \tag{17}$$

where $q_{d,m}^2 = \beta_0^2 - \epsilon_{d,m}$ and $\beta_0 = \sqrt{\epsilon_b\epsilon'_m/(\epsilon_b + \epsilon'_m)}$ is the dimensionless single-interface dispersion law of SPPs [rescaled to $(\omega/c)^{-1}$]. Note that the expressions above are directly related to the linear modes derived in Sec. II in the limit of small evanescent coupling and vanishing dielectric gain and metal loss.

B. Solvability condition and CMEs: $o(s^{3/2})$ order

At the $o(s^{3/2})$ order, the linearized Maxwell equations for the residual field $\Delta\mathbf{E} = (\Delta E_x \Delta E_z)^T$ yield

$$\hat{\mathcal{L}}_A\{\Delta\mathbf{E} + E_S[L\mathbf{e}_L + R\mathbf{e}_R]\} + E_S\hat{\mathcal{F}}[L\mathbf{e}_L + R\mathbf{e}_R] + -\chi_3 E_S^3[|L|^2 L\,|\mathbf{e}_L|^2\,\mathbf{e}_L + |R|^2 R\,|\mathbf{e}_R|^2\,\mathbf{e}_R] = 0, \tag{18}$$

where

$$\hat{\mathcal{F}} = \begin{pmatrix} -\Delta\epsilon - 2i\beta_0\partial_z & \partial_{xz}^2 \\ \partial_{xz}^2 & -\Delta\epsilon \end{pmatrix}. \tag{19}$$

Note that the linear operator,

$$\hat{\mathcal{L}}_A = \begin{pmatrix} \beta_0^2 - \epsilon_A & i\beta_0\partial_x \\ i\beta_0\partial_x & -\epsilon_A - \partial_{xx}^2 \end{pmatrix}, \tag{20}$$

does not coincide with the operators $\hat{\mathcal{L}}_{L,R}$. Indeed, $\hat{\mathcal{L}}_A$ depends on the complete dielectric permittivity profile ϵ_A, while $\hat{\mathcal{L}}_{L,R}$ depend on the isolated left and right single-interface profiles $\epsilon_{L,R}$. In turn, the linear $o(s^{1/2})$ order modes $\mathbf{e}_L, \mathbf{e}_R$ are not eigenvectors of the operator $\hat{\mathcal{L}}_A$, which accounts for the coupling terms between adjacent SPPs. Nonlinear BCs imply the continuity of $\mathcal{E}_z$ and $\epsilon_0\epsilon(x)\mathcal{E}_x + \mathcal{P}_{{\rm NL},x}$ at the interfaces $x = \pm a$ [retaining only $o(s^{3/2})$ terms]. Following the mathematical procedure reported in Refs. [37,38], we take the scalar product of Eq. (18) with the single-interface $o(s^{1/2})$ modes $\mathbf{e}_L, \mathbf{e}_R$. Nonlinear BCs enter the off-integral terms arising from integration by parts, which is applied to calculate the scalar products. Thus, coupling between adjacent SPPs is accounted for by the dimensionless coefficient [rescaled to $(\omega/c)^{-1}$],

$$\kappa = \beta_0\frac{\int_{-\infty}^{+\infty} dx\mathbf{e}_L^*(x)\cdot\hat{\mathcal{L}}_A\mathbf{e}_R(x)}{2\int_{-\infty}^{+\infty} dx\epsilon_A(x)|e_{R,x}|^2} = \frac{2\beta_0^3 e^{-2q_d a}}{\epsilon_b - \epsilon'_m}. \tag{21}$$

After taking the scalar products, one finds the CMEs for left and right SPPs as the solvability condition of the multiple-scale expansion:

$$i\frac{dL}{dz} = i\eta L - \kappa R - \gamma|L|^2 L, \tag{22}$$

$$i\frac{dR}{dz} = i\eta R - \kappa L - \gamma|R|^2 R, \tag{23}$$

where

$$\eta = \frac{\beta_0^3}{2}\left[\frac{\alpha(1 + i\delta)}{\epsilon_b^2(1 + \delta^2)} - \frac{\epsilon''_m}{(\epsilon'_m)^2}\right], \tag{24}$$

$$\gamma = \alpha\frac{(i - \delta)}{(1 + \delta^2)^2}\frac{\epsilon'_m\beta_0(q_d^2 + \beta_0^2)}{4q_d^2\epsilon_b(\epsilon_b + \epsilon'_m)}. \tag{25}$$

C. Loss-compensated nonlinear modes

In principle, the nonlinear stationary modes of the system can be thoroughly calculated under full-saturated conditions by numerically solving the full vectorial Maxwell equations [39]. However, CMEs are very useful to model optical propagation in plasmonic systems, as they enable the straightforward calculation of modes and can be numerically integrated rather easily. In Sec. II, we derived loss-compensated linear modes and their dispersion by neglecting the effect of gain saturation. Nonlinear CMEs derived in the previous section account for gain saturation in the approximation that the electric field is much smaller than the saturation field $|\mathcal{E}| \ll E_S$. If one wants to focus on the linear amplification regime, nonlinear effects can be artificially disregarded by setting $\gamma = 0$. In this case, the CMEs above thoroughly reproduce results of Sec. II in the limit of small coupling. Conversely, when nonlinear effects are retained, one can calculate the loss-compensated nonlinear modes of the plasmonic coupler by taking the Ansatz $L(z) = L_0 e^{i\Delta\beta z}$, $R(z) = R_0 e^{i\Delta\beta z}$, where L_0, R_0 are the complex mode amplitudes and $\Delta\beta$ is the correction to the unperturbed propagation constant β_0. Inserting the Ansatz above into Eqs. (22) and (23) one gets a nonlinear system of two complex algebraic equations in one real unknown $\Delta\beta$ and two complex unknowns L_0, R_0:

$$[-\Delta\beta - i\eta + \gamma|L_0|^2]L_0 + \kappa R_0 = 0, \tag{26}$$

$$[-\Delta\beta - i\eta + \gamma|R_0|^2]R_0 + \kappa L_0 = 0. \tag{27}$$

However, as the system above is invariant under an arbitrary constant phase transformation $L_0 \to L_0 e^{i\varphi}$, $R_0 \to R_0 e^{i\varphi}$, it is possible to set one amplitude to be real and without any loss of generality we set $L_0 \in \mathrm{Re}$. In turn, the system reduces to two complex equations (four real equations) in two real variables $\Delta\beta, L_0$ and another complex variable R_0 (two real variables). Thus, owing to the dissipative nature of our system, for every fixed set of parameters η, κ, γ, only a discrete amount of nonlinear modes exist. Symmetric and antisymmetric mode families can be calculated straightforwardly:

$$L_0 = \sqrt{\eta/\gamma''}, \quad R_0 = \pm L_0, \tag{28}$$

$$\Delta\beta = \pm\kappa + \eta'' + \eta'\frac{\gamma'}{\gamma''}. \tag{29}$$

Besides, in order to find further nonsymmetric solutions, we have numerically solved Eqs. (26) and (27) by using the Newton-Raphson method; results of our calculations are plotted in Fig. 4. In the panels of Fig. 4, we plot the dimensionless power density [rescaled to $(2\mu_0\omega)/E_S^2$]:

$$p_z = (|L_0|^2 + |R_0|^2)\frac{\beta_0\epsilon_b(\epsilon_b - \epsilon_m')}{2q_d^3 q_m^2}, \tag{30}$$

versus [Figs. 4(a) and 4(c)] the gain parameter α and [Figs. 4(b) and 4(d)] the semithickness of the dielectric slab a. The full dimensional power density is simply given by $P_z = E_S^2/(2\mu_0\omega)p_z$. Solid blue (dashed black) lines represent symmetric and antisymmetric (nonsymmetric) mode families. In our calculations we used the parameters $\epsilon_b = 1.8$, $\epsilon_m = -9 + 0.8i$; Figs. 4(a) and 4(b) $\lambda = 530$ nm, $\delta = 0$; and Figs. 4(c) and 4(d) $\lambda = 532$ nm, $\delta = -1$ [$\delta = T_2(\omega - \omega_R)$, for rhodamine 6G the resonant wavelength is $\lambda_R = 530$ nm, and the dephasing time is $T_2 = 80$ fs [40]]. For these parameters, the coefficients of the CMEs are $\kappa = 0.01$; Figs. 4(a) and 4(b) $\eta = 0.06$, $\gamma = 0.24i$; and Figs. 4(c) and 4(d) $\eta = 0.02 - 0.04i$, $\gamma = 0.06 + 0.06i$.

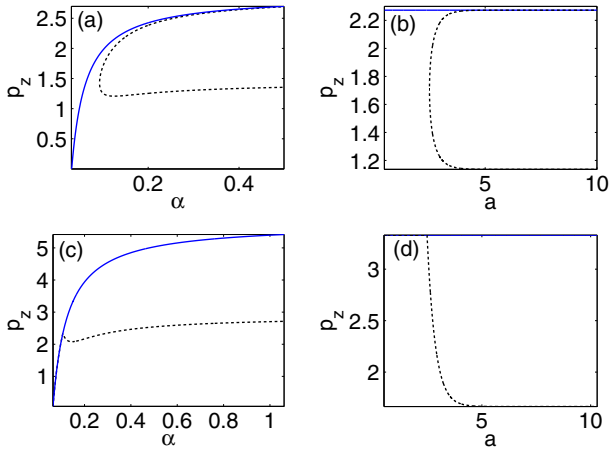

FIG. 4. (Color online) Families of dissipative nonlinear modes. Dimensionless power p_z versus (a) and (c) gain parameter α for $a = 3$, and (b) and (d) semithickness of the dielectric slab a for $\alpha = 0.15$. Solid blue lines represent families of antisymmetric and symmetric modes (which have the same power in the weak coupling regime considered here), while black dashed lines represent nonsymmetric mode families. In our calculations we used $\epsilon_b = 1.8, \epsilon_m = -9 + 0.8i$, (a) and (b) $\lambda = 530$ nm, $\delta = 0$, and (c) and (d) $\lambda = 532$ nm, $\delta = -1$.

We have studied the stability of these nonlinear stationary mode families under small perturbations by taking the Ansatz,

$$L(z) = [L_0 + \Delta L_1 e^{\mu z} + \Delta L_2^* e^{\mu^* z}]e^{i\Delta\beta z}, \tag{31}$$

$$R(z) = [R_0 + \Delta R_1 e^{\mu z} + \Delta R_2^* e^{\mu^* z}]e^{i\Delta\beta z}, \tag{32}$$

where $\Delta L_1, \Delta L_2, \Delta R_1, \Delta R_2$ are arbitrary small perturbations and $\mu = \mu' + i\mu''$ is the complex instability eigenvalue (the nonlinear mode is unstable when the real part of the instability eigenvalue is positive $\mu' > 0$). Inserting the Ansatz above in Eqs. (26) and (27) and linearizing with respect to the small perturbations $\Delta L_1, \Delta L_2, \Delta R_1, \Delta R_2$, one gets the linear eigenvalue problem $\hat{\mathcal{M}}\Delta L = \mu\Delta L$, where $\Delta L = (\Delta L_1 \Delta L_2 \Delta R_1 \Delta R_2)^T$ and we omit the cumbersome expression of the instability matrix $\hat{\mathcal{M}}$. We have numerically found the eigenvalues μ for every mode family, being able to determine their stability. We found that in the resonant case $\delta = 0$ [Figs. 4(a) and 4(b)] the symmetric and antisymmetric modes are marginally stable ($\mu' = 0$), while the nonsymmetric modes are always unstable. Conversely, in the down-detuned case $\delta = -1$ [Figs. 4(c) and 4(d)], the antisymmetric mode is always stable while the stability features of symmetric and nonsymmetric modes are more involved. Indeed, for every fixed semithickness parameter a, there exists a range of gain values where the symmetric mode is unstable (stable otherwise), while the nonsymmetric mode is stable only in a finite range of gain values above his onset threshold (unstable otherwise). For example, for $a = 3$ [see Fig. 4(c)] the symmetric mode (solid

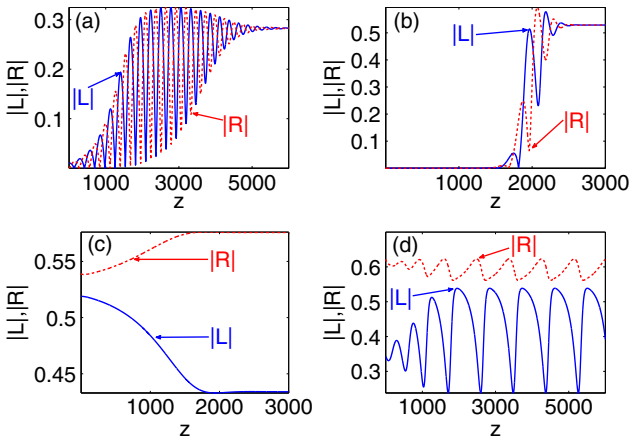

FIG. 5. (Color online) Propagation plots are as follows: z evolution of left $|L|$ (solid blue curves) and right $|R|$ (dashed red curves) amplitudes for the slab semithickness $a = 3$ and gain parameters (a) $\alpha = 0.072$, (b) and (c) $\alpha = 0.11$, and (d) $\alpha = 0.119$. In our calculations we used $\epsilon_b = 1.8$, $\epsilon_m = -9 + 0.8i$, $\lambda = 532$ nm, and $\delta = -1$.

blue line) is unstable within the range $0.071 < \alpha < 0.087$ (stable otherwise), and the nonsymmetric mode (dashed black line) is stable within the range $0.106 < \alpha < 0.120$ (unstable otherwise).

In order to validate our calculations and to verify the predicted stability features of nonlinear modes, we numerically integrated Eqs. (22) and (23) using a fourth-order Runge-Kutta algorithm. Results are depicted in the panels of Fig. 5, plotting the z evolution of left $|L|$ (solid blue curves) and right $|R|$ (dashed red curves) amplitudes for the slab semithickness $a = 3$ and gain parameter (a) $\alpha = 0.072$, (b) and (c) $\alpha = 0.11$, and (d) $\alpha = 0.119$. Our calculations were performed in the down-detuned case $\delta = -1$, where we assumed the same physical parameters used in Fig. 4. In Fig. 5(a) the gain parameter was set to $\alpha = 0.072$, where the nonsymmetric mode does not exist and the symmetric mode is unstable. The initial condition was set as a small perturbation of vacuum $L(0) = R(0) = 1 \times 10^{-3}$. Note that, after a propagation of about $z = 6000$, the system evolves to a stable antisymmetric state where $|L| = |R|$, in agreement with predictions of the linear stability analysis. In Figs. 5(b) and 5(c) the gain parameter was set to $\alpha = 0.11$, falling within the stability domain $0.106 < \alpha < 0.120$, where all modes (symmetric, antisymmetric, and nonsymmetric) are stable. In this case, the z evolution of the system highly depends on the input conditions. When the input condition is set as a small perturbation of vacuum, e.g., $L(0), R(0) \approx 10^{-3}$, we observe that the system evolves to a stable symmetric or antisymmetric state $|L| = |R|$ [see Fig. 5(b)], depending on the particular perturbation. Conversely, for a finite input condition far enough from the symmetric and antisymmetric modes, e.g., $L(0) = 0.52$, $R(0) = 0.54$, we observe that the system evolves to a stable nonsymmetric state $|L| \neq |R|$ [see Fig. 5(c)]. Besides, for gain parameters close to the upper edge of the stability domain $0.106 < \alpha < 0.120$, e.g., $\alpha = 0.119$ [see Fig. 5(d)], we observe that the system spontaneously evolves to a stable nonlinear oscillatory state with periodic oscillations in the optical amplitudes $|L|$, $|R|$. This scenario, resembling nonlinear beating in conservative couplers, is quite uncommon in dissipative systems such as the active plasmonic coupler considered in our calculations.

IV. CONCLUSIONS

In this paper we have investigated the propagation of surface plasmon polaritons in a metal-dielectric-metal plasmonic coupler. We have derived the loss-compensated nonlinear stationary modes of the system by developing a coupled-mode theory for the optical amplitudes. We have predicted the existence of a mode with broken symmetry for gain values higher than a characteristic threshold. We have studied the stability of symmetric, antisymmetric, and nonsymmetric modes by solving the linearized system for small perturbations and by numerically integrating coupled-mode equations in propagation. We found that the stability features of symmetric and nonsymmetric modes are involved in the down-detuned case. In particular, the nonsymmetric mode is stable only within a specific gain window. Within this particular gain range, we observe that the longitudinal evolution in the coupler highly depends on the input conditions, and that the system can evolve either to a symmetric, antisymmetric or nonsymmetric state or it can sustain stable oscillation cycles.

ACKNOWLEDGMENTS

This research is supported by the German Max Planck Society for the Advancement of Science (MPG). A.K. thanks the AvH Foundation for financial support.

[1] S. A. Maier, *Plasmonics: Fundamentals and Applications* (Springer, New York, 2007).
[2] E. Ozbay, Science **311**, 189 (2006).
[3] T. W. Ebbesen *et al.*, Nat. Lett. **391**, 667 (1998).
[4] J. B. Pendry, Phys. Rev. Lett. **85**, 3966 (2000).
[5] L. Novotny and N. van Hulst, Nat. Photon. **5**, 83 (2011).
[6] M. Kauranen and A. V. Zayats, Nat. Photon. **6**, 737 (2012).
[7] J. N. Anker *et al.*, Nat. Mater. **7**, 442 (2008).
[8] M. I. Stockman, Opt. Express **19**, 22029 (2011).
[9] E. Feigenbaum and M. Orenstein, Opt. Lett. **32**, 674 (2007).
[10] A. R. Davoyan, I. V. Shadrivov, and Y. S. Kivshar, Opt. Express **17**, 21732 (2009).
[11] C. Milian, D. E. Ceballos-Herrera, D. V. Skryabin, and A. Ferrando, Opt. Lett. **37**, 4221 (2012).
[12] A. R. Davoyan, I. V. Shadrivov, and Y. S. Kivshar, Opt. Express **16**, 21209 (2008).
[13] J. R. Salgueiro and Y. S. Kivshar, Appl. Phys. Lett. **97**, 081106 (2010).
[14] A. Marini, A. V. Gorbach, and D. V. Skryabin, Opt. Lett. **35**, 3532 (2010).
[15] A. R. Davoyan, I. V. Shadrivov, and Y. S. Kivshar, Opt. Lett. **36**, 930 (2011).
[16] J. R. Salgueiro and Y. S. Kivshar, Opt. Express **20**, 9403 (2012).

[17] W. Walasik, A. Rodriguez, and G. Renversez, Plasmonics **10**, 33 (2015).
[18] E. T. Arakawa, M. W. Williams, R. N. Hamm, and R. H. Ritchie, Phys. Rev. Lett. **31**, 1127 (1973).
[19] A. Marini and F. Biancalana, Phys. Rev. Lett. **110**, 243901 (2013).
[20] P. Berini and I. De Leon, Nat. Photon. **6**, 16 (2012).
[21] K. Leosson, J. of Nanophot. **6**, 061801 (2012).
[22] D. J. Bergman and M. I. Stockman, Phys. Rev. Lett. **90**, 027402 (2003).
[23] M. P. Nezhad, K. Tetz, and Y. Fainman, Opt. Express **12**, 4072 (2004).
[24] A. Ambati, S. H. Nam, E. Ulin-Avila, A. Genov, G. Bartal, and X. Zhang, Nano Lett. **8**, 3998 (2008).
[25] M. A. Noginov, V. A. Podolskiy, G. Zhu, M. Mayy, M. Bahoura, J. A. Adegoke, B. A. Ritzo, and K. Reynolds, Opt. Express **16**, 1385 (2008).
[26] P. M. Bolger, W. Dickson, A. V. Krasavin, L. Liebscher, S. G. Hickey, D. V. Skryabin, and A. V. Zayats, Opt. Lett. **8**, 1197 (2010).
[27] M. C. Gather, K. Meerholz, N. Danz, and K. Leosson, Nat. Photon. **4**, 457 (2010).
[28] A. Marini, A. V. Gorbach, D. V. Skryabin, and A. V. Zayats, Opt. Lett. **34**, 2864 (2009).
[29] A. Marini and D. V. Skryabin, Phys. Rev. A **81**, 033850 (2010).
[30] A. Marini, D. V. Skryabin, and B. Malomed, Opt. Express **19**, 6616 (2011).
[31] A. Marini *et al.*, New J. Phys. **15**, 013033 (2013).
[32] I. De Leon, J. E. Sipe, and R. W. Boyd, Phys. Rev. A **89**, 013855 (2014).
[33] R. W. Boyd, Z. Shi, and I. De Leon, Opt. Comm. **326**, 74 (2014).
[34] I. De Leon, Z. Shi, A. C. Liapis, and R. W. Boyd, Opt. Lett. **39**, 2274 (2014).
[35] B. Ung and Y. Sheng, Opt. Express **15**, 1182 (2007).
[36] A. A. Sukhorukov *et al.*, Opt. Lett. **39**, 462 (2014).
[37] D. V. Skryabin *et al.*, JOSA B **28**, 109 (2011).
[38] A. Marini, R. Hartley, A. V. Gorbach, and D. V. Skryabin, Phys. Rev. A **84**, 063839 (2011).
[39] Z. Adelpour *et al.*, JOSA B **31**, 1672 (2014).
[40] M. D. Barnes *et al.*, J. Chem. Phys. **97**, 7842 (1992).